Solar Energy 164 (2018) 109–118

Contents lists available at ScienceDirect

Solar Energy

journal homepage: www.elsevier.com/locate/solener

Simulator testing of evacuated flat plate solar collectors for industrial heat and building integration

R.W. Moss[a,*], P. Henshall[b], F. Arya[c], G.S.F. Shire[a], P.C. Eames[d], T. Hyde[c]

[a] School of Engineering, University of Warwick, Coventry CV4 7AL, UK
[b] Oxford Brookes University, formerly Centre for Renewable Energy Systems Technology, Loughborough University, UK
[c] School of the Built Environment, University of Ulster, UK
[d] Centre for Renewable Energy Systems Technology, Loughborough University, UK

ARTICLE INFO

Keywords:
Evacuated
Flat plate
Solar
Collector
Absorber
Efficiency

ABSTRACT

The concept of an evacuated flat plate collector was proposed over 40 years ago but, despite its professed advantages, very few manufacturers have developed commercial versions. This paper demonstrates the reduction in heat loss coefficient and increase in efficiency resulting from evacuating a flat plate collector: it is hoped that these results will stimulate interest in the concept. Evacuated tubes are now mass-produced in large numbers; evacuated flat plate collectors could in principle replace these tubes if the technical difficulties in creating extended metal-glass seals can be overcome. The experimental experiences described here should indicate targets for future research.

Two different designs of evacuated flat plate solar thermal collector, each with a 0.5 × 0.5 m flooded panel black chrome plated absorber, were tested under a solar simulator. The cover glasses were supported by an array of 6 mm diameter pillars. Inlet and outlet temperatures were monitored via PT100 RTDs and glass temperatures were measured using thermocouples. Inlet temperature was controlled by a fluid circulator connected to a header tank with a Coriolis mass flow meter to measure fluid flow rate. Testing was conducted indoors with and without the use of a fan to cool the top cover glass. The test conditions spanned the range $200 < G < 1000$ W/m^2, $0 \leqslant T_M \leqslant 52$ °C.

Evacuating the enclosure reduced the measured heat loss coefficient by 3.7 W/m^2 K: this was a close match to predictions and corresponds to an increase in aperture efficiency from 0.3 to 0.6 at $T_M/G = 0.06$ m^2 K/W. The poor efficiency under non-evacuated conditions was due to the black chrome absorber coating being less selective than commercial panel coatings.

The solder seals were developed from experience with vacuum glazing but the increased gap led to reliability issues. A vacuum pump maintained the enclosures under a high vacuum (<0.1 Pa) during testing. The enclosure based on a thin rear metal tray proved to be more effectively sealed than the more rigid enclosure with glass on both sides: the latter developed leaks as the front to rear temperature difference increased. The biggest challenge in the manufacture of evacuated flat plate collectors is to ensure a long-term hermetic seal such that no pumping is required.

1. Introduction

1.1. Evacuated flat plate solar thermal collectors

Evacuated flat plate (EFP) solar thermal collectors are anticipated to combine the high fill factor, ease of cleaning and visual aesthetics of flat plate collectors with the low heat loss coefficient of evacuated tubes. An array of ribs or pillars is required to support the glass cover against atmospheric pressure loading.

Such collectors can operate efficiently in low illumination conditions and moreover achieve “medium” to “high” delivery temperatures for industrial applications, a field that has recently attracted interest. The global potential for industrial use of solar heat is estimated as 180GW (ETSAP, 2015). The EU requirement for process heat in the 80–240 °C range has been estimated as 300 TWh per annum (Kalogirou, 2014) whilst in the United States process heat accounts for 38% of the total energy use (Riggs et al., 2017). Freeman et al. (2015) investigated the suitability of thermal collectors for small scale combined heat and power. Alobaid et al. (2017) compare the merits of thermal collectors and PV panels to power solar cooling systems. Absorption refrigeration systems are potentially a major market and require heat at 70–120 °C (Nkwetta and Smythe, 2012). Unlike concentrating collectors, EFP

* Corresponding author.
E-mail address: r.moss@warwick.ac.uk (R.W. Moss).

https://doi.org/10.1016/j.solener.2018.02.004
Received 14 December 2017; Received in revised form 29 January 2018; Accepted 1 February 2018

Nomenclature

A_A	frontal area of absorber
G	total (beam + diffuse) illumination (W/m^2) perpendicular to collector
T_a	ambient temperature
T_g	cover glass temperature
T_p	plate mean surface temperature
T_M	mean temperature difference $T_p - T_a$
T_M^*	scaled temperature difference T_M/G
U_L	overall heat loss coefficient (W/m^2 K)
c	specific heat of coolant (J/kg K)
c_g	specific heat capacity of glass (J/kg K)
d	absorber-glass gap (m)
h	heat transfer coefficient (W/m^2 K)
k	metal conductivity (W/m K)
$\dot{m}$	fluid mass flow rate
p	enclosure internal pressure (Pa)
r	radius (m) for radial conduction
w	glass mass/unit area (kg/m^2)
t_g	glass time constant (s)
η_A	efficiency based on absorber area
η_0,$\tau\alpha$	transmission-absorbance product

collectors can absorb diffuse light and operate without tracking the Sun.

The flat covers on EFP collectors are more attractive than bundles of evacuated tubes and, combined with the high efficiency, make them suitable for integration into roofs or building facias. The vacuum provides effective insulation between front and back covers in addition to its primary role in minimising heat loss from the absorber: evacuated collectors can therefore replace conventional insulation or vacuum-insulated panels (Alam et al., 2017). The use of a façade to generate heat may also be valuable (O'Hegarty et al., 2017; Leone and Beccali, 2016). Moss et al. (2018a) used a simulation based on weather data to show that evacuated flat plate collectors could be more efficient than other forms of solar collector for temperatures up to 210 °C.

There are currently two manufacturers of EFP collectors, SRB and TVP.

The SRB design (Benvenuti and Ruzinov, 2010) uses a long, thin format (64 cm wide, up to 3 m long) with an internal metal framework. The glass covers (front and back) are supported by longitudinal ribs; the absorber uses copper strips that sit between the ribs and are welded to a stainless tube. The edges of the glass are plasma-sprayed with a metal coating to facilitate soldering to the frame. The TVP design (Abbate, 2012; TVP datasheet) uses low melting point frit glass to seal the cover glass to a NiFe alloy edge spacer with a stainless steel back cover. The similarity in expansion coefficients between glass and this 48% nickel alloy avoids the shear stress peaks described by Henshall et al. (2014). The glass is supported by pillars passing through holes in the absorber.

Many proprietary details of these commercial collector designs are undocumented. The present investigation into theoretical and practical aspects of EFP collectors is intended to provide definitive data to guide future evacuated flat plate collector designs. The results presented here are novel in that they are the first published dataset to be accompanied by full construction details for the collectors.

Two different designs of experimental EFP collector were built, each using a flooded panel absorber but with different enclosures.

1.2. Collector efficiency research

Much research has taken place over the past 20 years to improve efficiency in conventional solar collectors.

Colangelo et al. (2016) reviews research into flat plate collectors over the past decade. An experimental comparison of flat plates and evacuated tubes is also given by Zambolin and Col (2010). There have been investigations into anti-reflection coatings (Helsch and Deubener, 2012; Caër et al., 2013) and heat transfer augmentation (Martın et al., 2011; Sharma and Diaz, 2011; Moss et al., 2017). Suman et al. (2015) provides a detailed overview of solar collector technology and configurations.

Collector efficiency is often characterised as $\eta = \tau\alpha - \frac{U_L T_M}{G}$. High temperature applications such as thermal power stations typically use concentrating collectors (Bouvier et al., 2016; Purohit and Purohit, 2017): these minimise the efficiency penalty at high T_M by effectively increasing the illumination intensity G.

An alternative approach for obtaining high efficiency at elevated T_M is to reduce the heat loss coefficient U_L. The radiative contribution to U_L is minimised using spectrally selective coatings and absorption media (reviewed by Kennedy, 2002); such coatings are now well developed.

In contrast, various approaches have been suggested to lessen the conduction component: this is a more intractable problem. Benz and Beikircher (1999) examined the possibility of using a low pressure (1–10 kPa) to inhibit convection together with krypton to reduce the conductivity. Buttinger et al. (2010) arranged a set of narrow concentrating trough collectors under a single cover glass. The internal pressure was reduced to 30 Pa to inhibit convective heat transfer. Beikircher et al. (2015) used a wide air gap to reduce conduction together with multiple intermediate glass or plastic films to inhibit convection. Ehrmann and Reineke-Koch (2012) used a double glazed cover glass. Brunold (SPF) describes a prototype collector using stacked 7 mm diameter glass capillary tubes as a thick transparent insulating layer that inhibits convection.

The use of a vacuum to eliminate conduction losses in a flat plate collector has been studied by Benz and Beikircher (1999) and Benvenuti and Ruzinov (2010), Benvenuti (2013a, 2013b). Under high vacuum conditions the molecular mean free path can exceed the typical separation d of components within the collector: the effective conductivity is then less than the nominal value. At pressure p and absolute temperature T the conductivity scaling multiplier k_p is a function of the Knudsen number Kn (Beikircher et al., 1996):

$$\mathrm{Kn} = \frac{0.008313}{\left(1 + \frac{116}{T}\right)pd},\quad k_p = \frac{k_{\mathrm{nominal}}}{1 + 3.75\mathrm{Kn}}$$

At a typical temperature of 320 K, $pd = 0.00255$ Pa·m is predicted to reduce the conductivity k_p to 10% of its normal level k_{nominal}. This is equivalent to 2.55 Pa for a 1 mm gap or 0.255 Pa for a 10 mm gap. Below this level of pd the effective conductivity is approximately proportional to pd (Collins et al., 1995), and the conductive heat loss will be proportional to $\frac{k}{d} \propto \frac{pd}{d} \propto p$.

The practical implementation requires low-outgassing materials (Moss et al., 2018b) and hermetic sealing of all joints. Commonly used flat plate collector materials such as flexible sealants are unsuitable for high vacuum conditions and the mechanical and thermal properties of alternative, vacuum-compatible materials introduce a number of design challenges.

2. Manufacture and instrumentation of evacuated collectors

2.1. Enclosure styles

Two styles of collector have been developed (Fig. 1): they share a common absorber design, mounted in different enclosures. In each case an array of pillars supports the cover glass against the atmospheric pressure load.

The "tray" style of enclosure uses a stainless steel tray with a single cover glass on the front (Henshall et al., 2014). This concept is intended

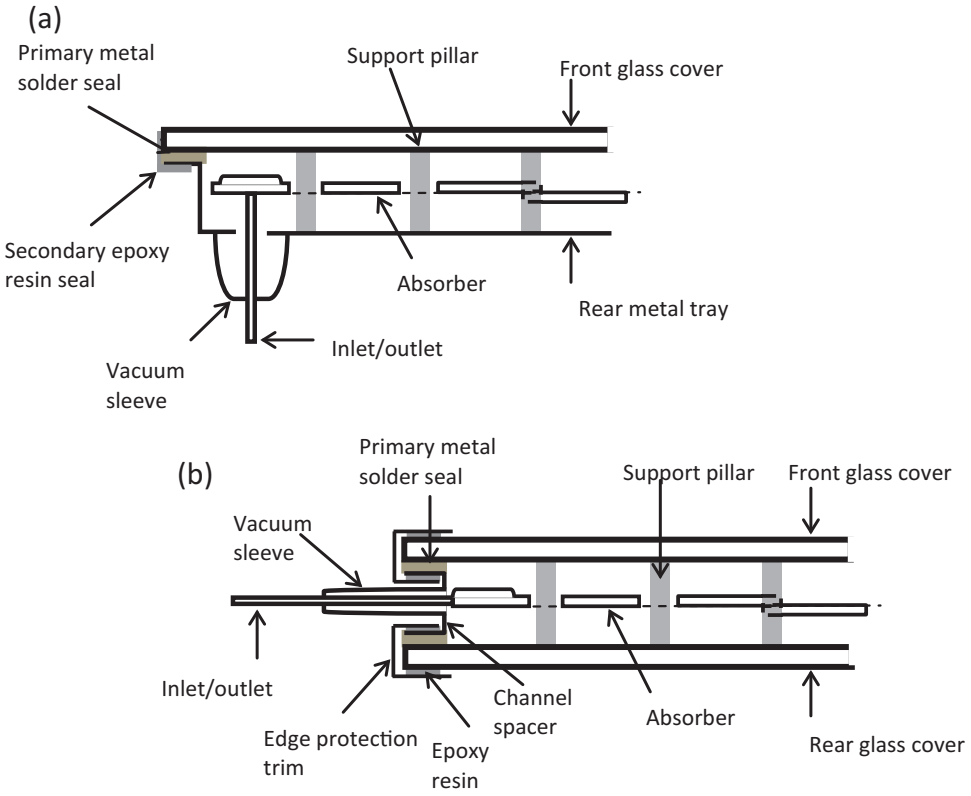

Fig. 1. Cross-sections of the collectors. (a) Collector P1 (with rear tray), (b) Collector F1 (symmetrical).

for industrial process heat applications where the visual appearance of the back face is not architecturally significant. The flexibility of the tray ensures that the pressure loading is shared equally over all the pillars even if the toughened glass is not absolutely flat. The pillars are spot welded to the tray: this holds them in the correct position and ensures they cannot come loose during fabrication or in service.

The "symmetrical" enclosure resembles a vacuum double glazing panel in that it has a sheet of glass to the rear as well as the front. The *U*-value is almost as low as for a vacuum glazing panel and the glass rear face makes its appearance suitable for architectural use in a building façade; it combines thermal insulation, heat collection and solar shading. This design is slightly heavier than the tray option and due to the rigidity of the glass any residual distortion after toughening (typically a slight "waviness" from the glass-handling rollers) will lead to unequal sharing of the pressure load between neighbouring pillars. This has not been a problem because the present configuration with 4 mm glass has a high safety factor. Further development of the pillars and manufacturing processes might allow the use of thinner glass or wider pillar spacing to give a more lightweight product.

Approximately 3% of the absorber area was taken up by the 49 through holes, Table 1, so only 97% of the "absorber area" actually absorbs heat. The ratio of absorber area/gross area was 84.5% for the tray enclosure and 68.3% for the symmetrical enclosure; this is lower than the typical 89% for commercial flat panels, which typically have similar edge widths of 13–35 mm (SPF, 2017) but are usually 2 m^2 or more in area. Full size evacuated flat panels should therefore not suffer a significant fill factor penalty relative to conventional panels.

Table 1
Design and test parameters.

Aperture area	0.47 m× 0.47 m= 0.221 m^2
Gross area	0.49 m× 0.49 m= 0.24 m^2 (tray)
	0.52 m× 0.52 m= 0.27 m^2 (symmetrical)
Glass thickness	4 mm
Pillar length	25 mm
Pillar diameter	6 mm
Pillar array pitch	60 mm
Absorber through-hole diameter	13 mm
Heat transfer fluid specific heat capacity (J/kg K at 30, 80 degC)	4180–4200 (water + inhibitor)
	3640–3840 (Tyfocor-LS)
Typical test flow rate	2–6.4 g/s (median 4 g/s)
Typical inlet to outlet fluid temperature rise	−1.8 to +7.4 °C (median 3 °C)

2.2. Absorber manufacture

2.2.1. Configurations and coatings

Both designs of collector used similar absorbers, the only difference being the inlet and outlet pipework. Following initial investigations (Moss and Shire, 2014; Moss et al., 2017) into micro-channel and serpentine tube absorbers a flooded absorber design was chosen. 0.7 mm T316 stainless steel sheets are hydro-formed and TIG welded to a 0.9 mm baseplate (Moss et al., 2018b), then water-bath tested for leaks using helium at 1.4 bar gauge. An array of through holes allows the glass support pillars to pass through the absorber without making contact, Fig. 2. The internal height is typically 2 mm, increasing to 3.5 mm near the intake and outlet connections.

Having largely eliminated gaseous conduction losses, the main heat loss mechanism is radiative transfer between absorber and cover glass. Many selective coating options were investigated including commercial solar panel coatings, black solar panel paint (Solkote®), black nickel (Lira-Cantú et al., 2005; Lizama-Tzec et al., 2015) and black chrome plating, sol-gel (Joly et al., 2013) and PVD coatings (Selvakumar and Barshilia, 2012; Gao et al., 2017).

Commercial coatings after many years' development now offer emissivities as low as 0.04. Four manufacturers were approached but none were able to apply their coatings on a one-off basis to a welded steel absorber.

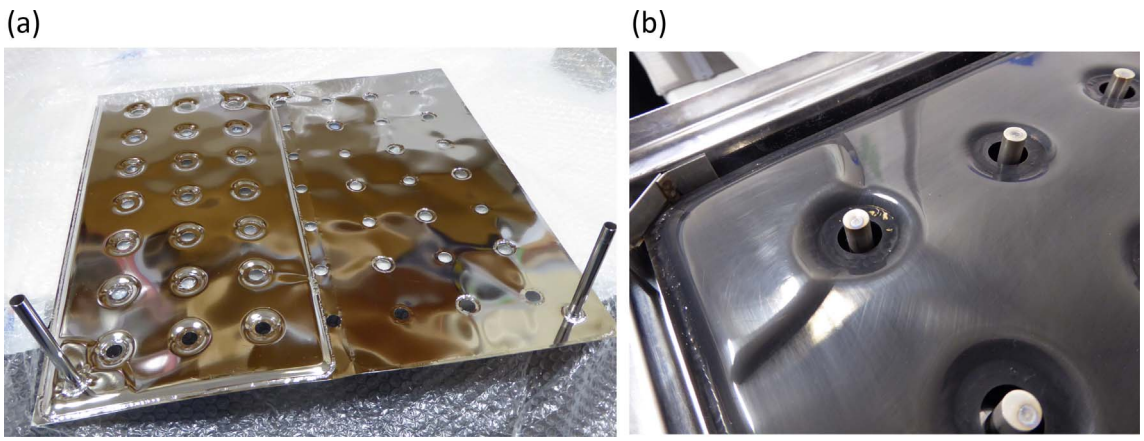

Fig. 2. (a) Absorber after TIG welding and electro-polishing to prepare for black chrome plating. This view of the underside shows the perpendicular feed tubes that pass through a stainless steel tray forming the rear of the enclosure. (b) Black chrome plated absorber in a stainless tray prior to soldering the cover glass in place.

Black chrome plating was widely adopted as a spectrally-selective surface for solar panel use in the 1970's (McDonald, 1975) because it was more durable in hot and humid conditions than black nickel. Two local black chrome suppliers were used. Chromium plating suffers from a highly non-linear relationship between electric field strength and deposition rate: in each case it proved very difficult to obtain a sufficiently uniform coating, particularly when moving from small samples to the full size absorber. The coating typically achieved an absorbance of 0.95 or higher, where black, but attempts to keep the emissivity low often resulted in some patches with only a minimal deposit.

Emissivity was measured over an 8 × 8 grid using an R&D Systems AE1 emissometer and was found to have considerable non-uniformity. The emissivity was generally higher than planned but was the best that could be achieved using local suppliers with general purpose plating as opposed to specialist solar panel equipment. Attempts to reduce the emissivity using lower current density or shorter plating time led to significant areas without any black coating.

2.2.2. Parasitic heat losses

One potential problem when using pins to support the glass is that thermal expansion could close the gap between absorber and pins leading to a thermal bridge. The expansion coefficient of 316 stainless is 16×10^{-6} K^{-1}. Using 6 mm diameter pins in 13 mm diameter holes and assuming no initial misalignment, the gaps towards the ends of the panel would close for a centrally-held 2 m long absorber if it were 219 °C hotter than the cover glass. Longer absorbers or panels operating at higher temperatures would require the pins to be initially located closer to the other side of the hole, higher initial clearance, or slots.

The flow and return tubes were thermally isolated from the tray and edge seal by thin-walled 304L stainless steel sleeves (Figs. 1 and 4 below). The symmetrical enclosure for instance used tubes of length 85 mm, outer diameter 17.5 mm and wall thickness 1.25 mm giving a conductance for each sleeve of 0.012 W/K. When operating at T_M = 50 °C the heat loss through both sleeves would be 1.2 W and would reduce the efficiency by 0.0054 at G = 1000 W/m^2. Radiative loss inside the sleeve has been assumed negligible since both surfaces have low emissivity. This conduction loss is an overestimate since in practice the thermal resistance will include contributions from the surrounding tray or edge seal.

There is also a thermal conduction path via the absorber supports. Fig. 2(b) shows the bracket at each corner of a tray enclosure. These brackets support the weight of the absorber whilst allowing thermal expansion. The absorber touches the edge of a 0.9 mm thick stainless strip. The low conductivity of stainless steel and the point contact provide a thermal resistance sufficiently high to have little impact on the efficiency. An estimate of the conductivity may be obtained by modelling the sheet around a contact point using the standard hollow cylinder formula for radial conduction: $\dot{Q}' = -2\pi \frac{k(T_2 - T_1)}{\ln\left(\frac{r_2}{r_1}\right)}$ W/m of plate thickness (Incropera and DeWitt, 2002).

Very conservative estimates of the heat loss, assuming a contact region of length 1 mm above and below each corner, suggest that the overall efficiency loss would be only 0.007 at G = 1000 W/m^2, T_M = 50 °C.

The symmetrical enclosure used the coolant tubes to locate one side of the absorber. The other side was supported top and bottom by a stainless steel bracket and PTFE pin (visible in Fig. 4(b) below). The low conductivity of PTFE (≈0.25 W/m K) and need for only two supports leads to a much lower efficiency penalty of order 0.0003 at the same conditions.

3. Test facility and instrumentation

3.1. System components and test procedure

A dedicated solar simulator was designed and built for evacuated panel testing (Moss et al., 2018c), Fig. 3(a). Four 400 W halogen floodlights provided illumination; the light was directed down through a reflecting box to generate multiple virtual images and achieve uniform illumination without an extensive array of lamps. The illumination level was controlled by a variable transformer. The simulator illumination was calibrated against input power using a Kipp and Zonen CM P-11 pyranometer. The electrical power was measured throughout each test using a Hameg 8115 power meter.

A number of heat transfer fluids were used: water with a corrosion inhibitor (initially Fernox *F1*, later Fernox *MBK*) and Tyfocor-LS, a glycol-water solar panel coolant. A circulating bath heated the coolant to the desired test temperature and pumped it up to a header tank from where it flowed under gravity through the absorber and a Coriolis mass flow meter, Fig. 3(b). Flow temperatures were measured by Pt100 RTDs, two at absorber inlet and two at outlet, Fig. 4(a). Glass temperatures were measured using thermocouples bonded to the glass, Fig. 4(b) (Moss et al., 2018c).

The vacuum system used an Edwards 18 two stage roughing pump and a Speedivac E04 diffusion pump. Pressures were measured using a kJ Lesker combined vacuum gauge.

Type *T* thermocouples and Pt100 RTDs were used. Thermocouples were connected directly to a Measurement Computing HS1616-USB data acquisition system. The RTDs were connected via Weidmuller signal conditioning blocks, with each RTD always using the same block, and were calibrated with cold and hot water in an insulated beaker prior to use. A pair of RTDs was used at both inlet and outlet to reduce uncertainty and to check for transducer drift.

Two collectors were tested: "P1" (tray) and "F1" (symmetrical).

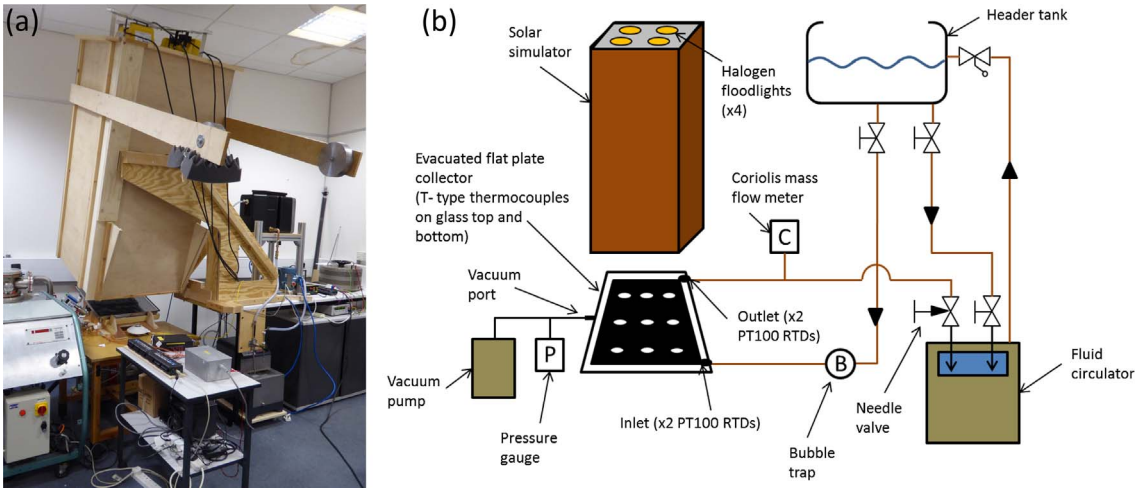

Fig. 3. Experimental facility (a) Photograph showing scale of components, (b) Schematic diagram.

Both collectors successfully demonstrated a significant efficiency improvement when evacuated. During testing the collectors were supported by a 50 mm think sheet of polyurethane foam insulation to minimise any uncertainty regarding heat losses from the rear.

A circulating bath was used to circulate heat transfer fluid through a header tank at temperatures up to 80 °C. Once the header temperature was steady, coolant was allowed to flow under gravity through a bubble trap, the collector, a Coriolis mass flow meter and a needle valve before returning to the bath. The collector was inclined at 16.5° to the horizontal so that, in the event of any bubbles forming inside, the bubbles would merge and flow through instead of covering the upper surface. The header tank took 1–2 h to reach steady state so testing over the course of a day generally explored a range of illumination levels at a single flow temperature. The absorber time constant was of order 2 min and outlet temperature would largely stabilise about 6 min after changing the illumination. There was however a much slower effect due to the response of the tray and glass.

3.2. Test stability and instrumentation accuracy

The test data was collected on eight separate days. During each day, the flow temperature was held constant but the illumination level was set to a number of different levels. The flow rate was chosen to allow accurate measurement of the temperature rise through the absorber rather than to minimise the temperature rise in the search for the greatest possible efficiency. Typical flow rates were in the range 3–6 g/s and the median change in fluid temperature was 3.4 °C, Fig. 5.

Prior to testing the water bath temperature was set to closely match the room temperature and water was circulated with an insulating sheet covering the collector. This enabled a datum adjustment, if necessary, to ensure all four inlet and outlet RTDs started at the same temperature. Since the heat flux was calculated from the difference in temperature between the flow inlet and outlet RTDs the absolute accuracy of each RTD was less important than any possible drift during the test period. Platinum RTDs typically have a stability standard of ± 0.1 °Cper year so the maximum expected divergence of two RTDs is of order 2×10^{-4} °C over an 8 h test period.

After setting each illumination and flow condition, testing continued until RTD and thermocouple signals appeared sufficiently stable that significantly different values could not be expected were the test to be continued, within a practical time frame. The initial time constant of the absorber outlet temperature in response to flow or illumination changes was of order 2 min; the glass covers however have a longer time constant of order 1 h. Stability was assessed by curve fitting the data at each condition to determine the magnitude of the gradient. For the data points in Fig. 10 (below), the stability parameters were:

- mean absolute change in heat flux 0.6% per minute
- mean absolute change in top glass temperature 0.14 °C per minute
- mean absolute change in lower glass temperature 0.08 °C per minute

Coriolis meters are typically accurate to better than 0.1% of liquid flow.

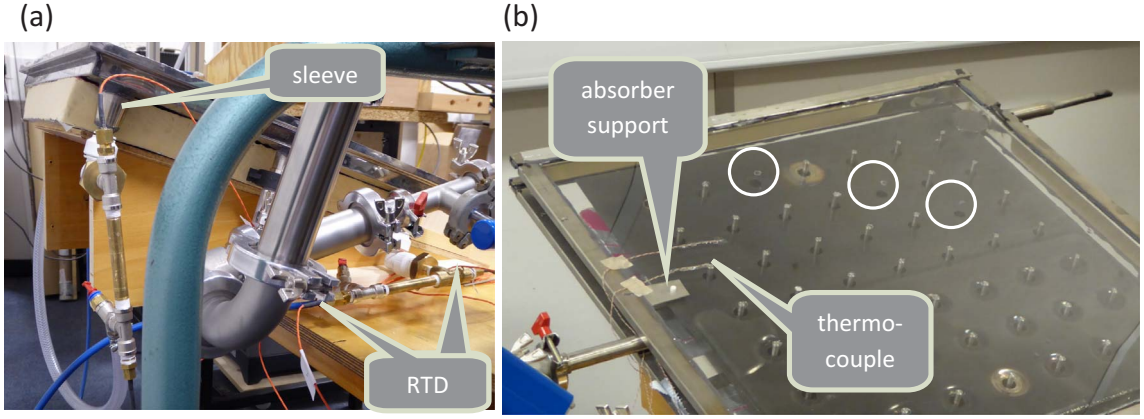

Fig. 4. (a) Tray collector "P1" showing RTDs to measure flow temperature. Inlet is on the right here. Pipes were insulated prior to testing. (b) Symmetrical collector "F1" showing top glass thermocouples; the lower glass is instrumented similarly. The two bare regions result from plating conductors being bolted to these holes. Circles show where pillars are missing.

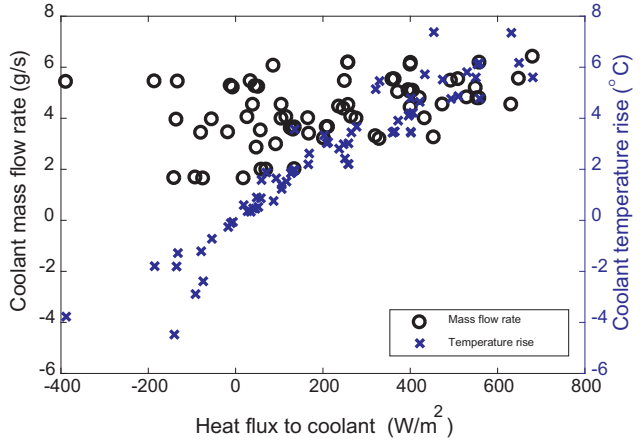

Fig. 5. Coolant flow rates and temperature rise through the absorber. Negative heat flux indicates heat loss exceeding the radiation absorbed.

3.3. Cover glass temperature effects

Heat flux to the cover glass was higher than might be expected in a commercial collector operating outdoors. The increased heat transfer is due to the absorber emissivity being considerably higher than might be possible with a state of the art coating and also, for the top cover glass, the result of long IR wavelengths being absorbed by the glass (Moss et al., 2018c). Heat transfer from absorber to glass is evident during the pre-test warm-up period, Fig. 6; in this test the enclosure was insulated top and bottom to show the effect of internal heat transfer. Fig. 6 also shows a period with the fan turned on to confirm that the pipework was sufficiently insulated and draught-proofed.

The time constant of the glass results from its heat capacity and the heat transfer coefficients on each side; it can be calculated as $t_g = \frac{wc_g}{h}$ and is approximately 1 h for the bottom glass. Ideally test conditions should be held stable for perhaps 4 time constants to bring the temperature differences to within a fraction $e^{-4} \approx 0.018$ of their final value. This condition could not be achieved in the course of a day's testing with a number of illumination levels; instead, data capture proceeded until the rates of change were deemed sufficiently low as described in Section 3.2 above.

A simulation was performed to assess how closely the experimental data set matched conditions that would occur if the experimental panel on its foam base had been installed outdoors and had reached steady-state conditions in sunlight. It indicated that under sunlight and high vacuum conditions, with no wind, the top and bottom glass covers should eventually reach a temperature:

$$T_{g,top} \approx T_a + 0.4T_M,\ T_{g,bottom} \approx T_a + 0.75T_M$$

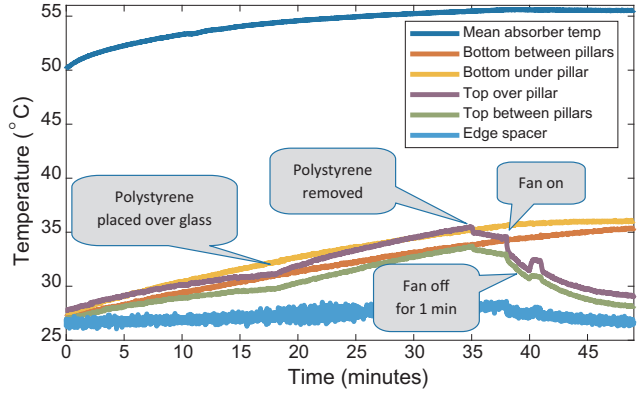

Fig. 6. Typical warm-up history of glass due to hot water flow through the absorber. No illumination, F1, 0.019 Pa.

The simulation code (Moss et al., 2018a) uses a heat balance model to determine the glass temperature for a given absorber temperature. This prediction used the measured absorber emissivities, assumed natural convection, neglected thermal bridging via the pillars and edge spacer and omitted the simulator's long wavelength IR effects.

For comparison with these glass temperature predictions the experimental thermocouple readings were fitted using a linear equation $T_{g,i} = T_a + a_i + b_i T_M + c_i G, i = 1,2$. The Pearson correlation coefficient in terms of G for the lower glass is however only 0.07: as expected, the illumination has little consistent effect on lower glass temperature. The other correlation coefficients ranged from 0.65 to 0.93.

The best fit values for the 41 evacuated, fan-cooled data points were:

- Top glass $(a,b,c) = (-0.8,0.131,0.0061)$
- Bottom glass $(a,b) = (-0.73,0.45)$, setting $c_2 = 0$ because of the very weak G correlation.

Both glass temperatures are cooler than the steady-state, open air simulation implies: the experimental efficiencies are therefore slightly lower than would be expected if the collectors were tested outdoors. The top glass temperature will differ from the simulation both because of IR absorption and the draught from the cooling fan: the $b_1 = 0.131$ coefficient (as opposed to the predicted 0.4) shows that the fan has cooled the glass below the expected outdoor level. The lower glass with $b_2 = 0.45$ compared to the predicted 0.75 also did not reach the predicted temperature. This may in part be due to its long time constant. The thermocouple temperatures are however point measurements taken 80 mm from the edge of the enclosure and are not necessarily typical of the surface average temperature: the variation in coating emissivity over the absorber surface implies that temperature variations across the glass are to be expected.

3.4. Initial testing

Initial testing showed that the cover glass temperature rose to over 50 °C under the solar simulator. This was unexpected because high transparency, low iron glass had been used in both collectors. Subsequent investigation showed there to be a long wavelength (>3000 nm) infra-red component of the floodlight spectrum. At these wavelengths glass is opaque; this spectral component was therefore absorbed by the glass instead of passing through to the absorber. The glass dome on the pyranometer also blocked this radiation so the pyranometer reading was broadly representative of the radiation impinging on the absorber plate. Simulations (Moss et al., 2018c) suggest that the efficiency with this illumination spectrum is approximately 1% higher than the efficiency under a nominal AM1.5 solar spectrum, if the efficiency is based on the pyranometer power reading and there is no change in cover glass temperature.

Two kinds of efficiency test were carried out: (a) under ambient conditions, (b) with a fan blowing air over the collector to limit the glass temperature. The latter case gives a better indication of efficiency since power in the long wavelength component which cannot be measured by the CMP-11 pyranometer is then removed to the environment instead of raising the glass temperature and reducing the heat losses from absorber to glass.

3.5. Enclosure mechanics

Initial attempts to fabricate trial specimens for the symmetrical enclosure using non-toughened glass always suffered from fracture of the glass during cool-down after soldering. The fracture problem was ultimately overcome using toughened glass.

Stress analysis (Henshall et al., 2016) suggested that 4 mm glass supported by an array of 6 mm diameter pillars at 60 mm pitch would result in acceptable stress levels for toughened glass under vacuum

loading. The stresses and deformations due to thermal expansion in vacuum glazing have been investigated by Simko et al. (1998): he found that temperature differences between front and back cause the panel to adopt a spherical curve. This deformation results in high stress levels near the glass edges where the bond line effectively increases the thickness and stiffness.

A further consideration is that the glass toughening process causes slight distortion in the form of a ripple (Henshall et al., 2016). The tray-based enclosure had sufficient flexibility to accommodate these ripples and distribute the pressure load uniformly over the pillars.

The symmetrical enclosure with glass on both sides was much stiffer. Any ripple in the glass would have caused uneven load sharing between pillars when evacuated. Pillars were located on the bottom glass by the smallest possible drop of silicone rubber. Collectors designed to maintain their vacuum under long-term sealed conditions could not however use an adhesive with any out-gassing risk: they might instead require a network of thin wires or mesh to maintain pillar positions before suck-down.

When the solder melted in the oven the glass settled until supported by the pillars. Three pillars were accidentally dislodged and are now loose inside the enclosure. The vacant pillar locations are shown in Fig. 4(b). This enclosure successfully withstood evacuation to <0.1 Pa during the test period which indicates that an enclosure with the pressure load evenly distributed over a full complement of pins would have a considerable safety margin. Further development could lead to a lighter design using thinner glass or allow more widely-spaced pillars: the latter would also simplify absorber manufacture.

3.6. Vacuum sealing

Continual pumping was required to maintain a sufficiently low pressure. Some outgassing of experimental components was expected since it was not feasible to either bake-out the assembly after soldering or bake the components and keep in an inert environment throughout the soldering and instrumentation processes.

The rate of pressure rise in the symmetrical enclosure however suggested some leakage through the solder seal. The pressure maintained by the diffusion pump increased in steps as the solder seal degraded (Fig. 7): it appears that differential expansion due to temperature differences between the front glass, edge seal and back glass caused shear stresses in the solder joint (Henshall et al., 2016). Temperature differences as high as 17 °C were experienced during initial testing without a cooling fan. A practical solar collector providing building insulation might have to withstand differences in air temperature of 30 °C or more between outdoor and indoor environments and it is crucial to the longevity of the panel that it should withstand any such thermal stresses.

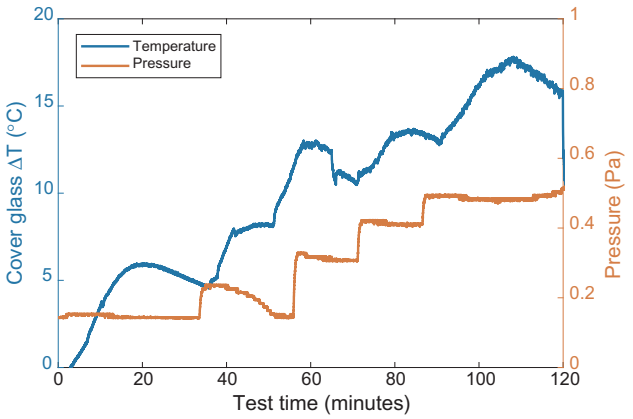

Fig. 7. Leak development history (symmetrical enclosure). Glass temperature (mean difference between thermocouples on top and bottom covers) varies here in response to changes in illumination and flow rate. The collector was subsequently resealed using epoxy resin.

Even with closely matched thermal expansion coefficients, the difference in temperatures between top and bottom cover glass will cause differential expansion. A full-size panel with soda-lime glass covers 2 m long would develop a length difference of 0.5 mm at $\Delta T = 30$ °C relative to isothermal conditions unless the bond line could develop sufficient shear stress to counteract the thermal growth. Conventional flat panels can use flexible sealants to allow expansion but no currently available flexible sealant has sufficiently low out-gassing rates for use in a sealed-for-life evacuated panel.

Solutions to this might include use of low expansion borosilicate glass and the development of a flexible metal edge spacer that could accommodate the relative movement of the glass.

To determine whether these leakage steps originated from the edge seal or the absorber the solder seals were thoroughly coated with Permabond MT382 and ET530 epoxy resins. This significantly reduced the leakage, indicating that the leaks were through the solder joint, and enabled testing to resume. A pressure rise rate of 0.29 Pa/h was achieved after resealing, with the isolator valve closed, but the leakage rate gradually rose again during subsequent testing.

Two types of solder were evaluated while developing the enclosures. The principal factor in the choice of Cerasolzer 217 in place of S-Bond 220 was its lower melting point (217 °C versus 240–260 °C). The low melting point reduces stresses due to differences in expansion coefficient between glass and steel as the enclosure cools after the glass and edge seals are fused together.

Previous experience in fabricating vacuum glazing samples using indium had successfully achieved a hermetic seal and survived hot-box testing; similarly, a trial symmetrical enclosure survived a difference in glass temperatures of 13.7 °C in the hot box. The 17 °C difference when simulator testing slightly exceeded this previous limit. The leakage experienced with the current panels might also be a result of using Cerasolzer instead of indium or it might reflect the difficulty of forming a hermetic seal against stainless steel using ultrasonic soldering techniques to disrupt oxide layers. It seems probable that thermal stresses are generated both by temperature gradients within the structure and by a mismatch in thermal expansion coefficients between the 304-series stainless edge spacer and the soda-lime glass: these cause a gradual deterioration in the sealing performance of the soldered joint.

4. Test results

4.1. Results for the tray enclosure

The “tray” collector was tested first. During initial testing with hot water circulating through the absorber the heat losses were measured while reducing the enclosure pressure, Fig. 8.

There was no illumination so the net heat flux into the collector was negative (i.e. a heat loss from absorber to cover glass). At approximately 57.5 min into the test, the pancake valve to the diffusion pump was opened and the pressure in the enclosure fell rapidly to <0.1 Pa. At this point the level of heat loss reduced significantly. The improvement in the heat loss coefficient supports the prediction that conduction is reduced by at least a factor of 10 when $pd < 0.00255$ Pa·m.The efficiency was measured both at ambient pressure and when evacuated, Fig. 9. To maintain the highest accuracy in the measurements, a water temperature of approximately 80 °C was used and a wide range of T_m^* was achieved by varying the illumination level G. Efficiency has been calculated in terms of the heat flux to the coolant, the absorber area and the illumination:

$$\eta_A = \frac{\dot{m}c(T_o - T_i)}{GA_A}$$

A_A is the area of the black chrome plated absorber; to allow sensible comparison with non-vacuum panels, the area of the through-holes has

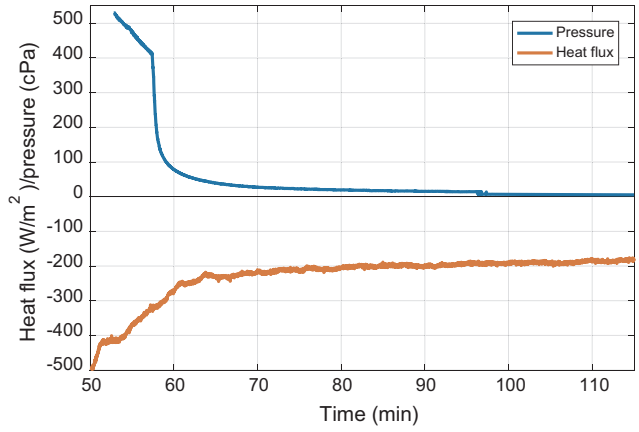

Fig. 8. Rapid reduction in heat losses observed as pressure fell below 0.1 Pa.

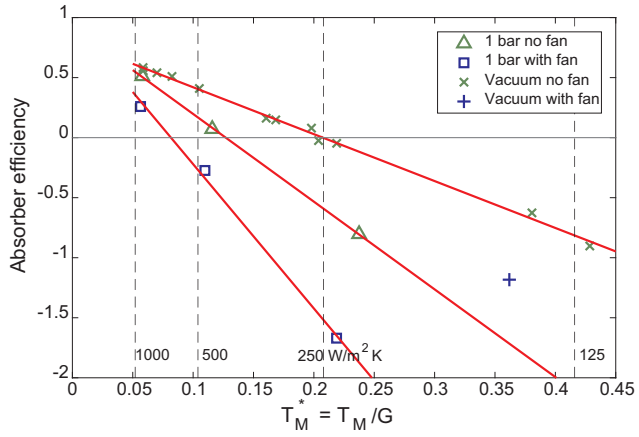

Fig. 9. Collector P1 test results, showing effect of cooling fan. Line fits (through all available data points) included for clarity.

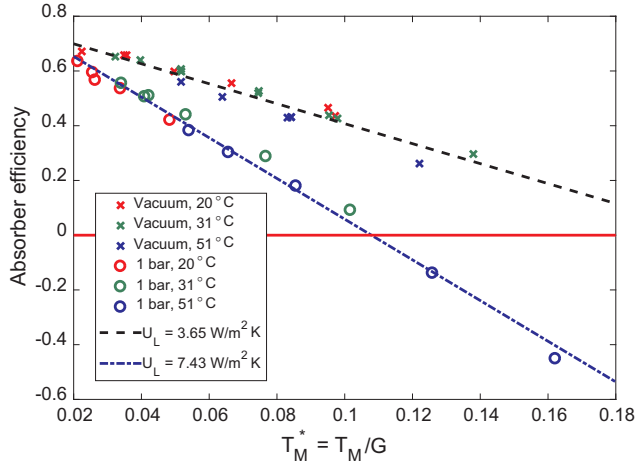

Fig. 10. Symmetrical collector (F1) using water + corrosion inhibitor. 95% confidence limits for U_L: [3.52, 3.78] and [7.02, 7.85] based on line fit statistics.

not been subtracted from the total. These results were obtained with a water inlet temperature in the range 70–80 °C, giving $T_M \approx 52$ °C; the illumination was varied to achieve different values of $T_m^* = \frac{T_M}{G}$. The heat loss coefficient U_L typically rises slightly with T_M, because it depends on radiative and convective heat loss mechanisms, but is expected to be independent of the illumination level G.

The absorber efficiency is commonly characterised as

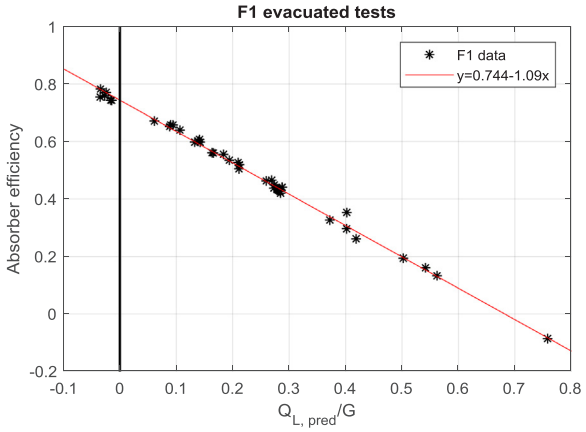

Fig. 11. The total heat loss is 1.09× the radiative prediction based on absorber and glass temperature data.

$\eta_A = \tau\alpha - \frac{U_L T_M}{G} = \tau\alpha - U_L T_m^*$. Testing at constant T_M (constant U_L) is therefore expected to give a straight line of gradient $-U_L$ on the η_A versus T_M^* graph.

Least squares lines have been fitted through three of the data sets. The fourth case "Vacuum with fan" was found after de-rigging in preparation for the F1 tests to have only one data point with sufficient temperature stability to give accurate values.

The efficiency improvement between the "1 bar" and "Vacuum" conditions is evident. The intercept with the zero efficiency line shows the reduction in critical radiation level achieved under evacuated conditions. Below this line tests with very low illumination levels produced negative efficiencies because, with hot water circulating at $T_M \approx 52$ °C, the radiative heating was less than the heat loss. A low critical radiation limit is important for installations since it reduces the heat loss from the system during periods of weak insolation.

The fan allows the cover glass to act as a "cold sky" filter, giving efficiencies comparable with AM1.5 solar spectrum conditions at the same cover glass temperature; without a fan the efficiency is over-estimated because the long-wavelength IR component is not included in the pyranometer measurement of illumination. The long wavelength component is thought to contribute approximately 14.5% over and above the pyranometer reading.

The P1 evacuated data is consistent with heat balance models using a mean coating absorbance of 0.9 and mean emissivity of 0.52. This is a much higher emissivity than would be expected in a commercial panel. The high level of heat transfer between absorber and cover glass (illustrated by the warm-up curves in Fig. 6) means that even without an IR spectral component the cover glass would be significantly hotter than ambient.

The difference in efficiency between the "1 bar no fan" and "1 bar with fan" lines in Fig. 9 illustrates the sensitivity of a conventional flat plate to ambient conditions. The line gradient U_L is a function of heat transfer coefficients from absorber to glass and from glass to environment: the fan increases the glass-to-environment coefficient with the result that U_L increases from 7.3 to 12.0 W/m^2 K under 1 bar conditions. Conversely with no fan, evacuating the enclosure reduced U_L from 7.3 down to 3.9 W/m^2 K.

Simulations (Moss et al., 2018a) with the absorber held at $T_M = 52$ °C (AM1.5 spectrum, $G = 1000$ W/m^2, evacuated, no fan) suggest that the steady state upper glass temperature would be 21 °C above ambient due to radiative heat transfer from the absorber. Experimentally, during tests with the fan on the upper glass was typically cooled to 12 °C above ambient leading to increased heat loss from the absorber. The "with fan" efficiencies are therefore slightly lower than would be expected if the simulator had a separate cold sky filter to achieve the correct spectrum without using a fan.

4.2. Test results for the symmetrical enclosure

4.2.1. Testing with water

This absorber was tested over a wider range of conditions, with multiple fluids. Most tests used a cooling fan to limit the glass temperature as described in Section 3. Initial testing used water with a central heating additive, Fig. 10.

The fact that the vacuum and non-vacuum tests each lie close to a best-fit straight line indicates that U_L did not change significantly over the testing range of fluid temperatures, T_M = 20, 31 and 51 °C.

These U_L mean heat loss coefficients are higher than commercial standards because of the poor emissivity of the black chrome plating. The difference between the 1 bar and evacuated U_L values, 3.7 W/m^2 K, does however demonstrate the reduction in heat losses possible in an evacuated system.

4.2.2. Testing with Tyfocor-LS

Following the water + MBK tests, some tests were repeated using Tyfocor-LS as the coolant to check the accuracy and repeatability of the efficiency readings. The results were very similar. Best fit lines, comparing only high vacuum data taken at T_M = 52 °C gave:

- $\eta_A = 0.779 - 4.205 T_M^*$ with water + MBK (6 data points, $0.052 < T_M^* < 0.122$)
- $\eta_A = 0.759 - 3.596 T_M^*$ with Tyfocor-LS (7 data points, $0.052 < T_M^* < 0.4$)

The Tyfocor U_L value is very close to the 3.65 W/**m^2 K** obtained for water + MBK using the full set of temperature points. The 4.205 W/m^2 K for the 52 °C water tests is probably less accurate due to the small range of T_M^* covered. There is also some test to test variation resulting from changes in rear glass temperatures over the course of each day's testing.

4.2.3. Comparison with predicted heat losses

Uncertainties resulting from test to test variations and transient effects on glass temperature can be eliminated by predicting the absorber heat loss based on measured absorber and glass temperatures.

The combined emissivity of glass and absorber is given by $\varepsilon_{ag} = (\varepsilon_a^{-1} + \varepsilon_g^{-1} - 1)^{-1}$. A parallel plate formula is used because the gap is much smaller than the width. This absorber has an estimated mean emissivity of 0.385 (top), 0.15 (bottom): the underside has a minimally plated region which would have made the absorbance too low for use facing upwards. Assuming a long wavelength emissivity of 0.96 for the glass the total radiative heat flux from the absorber to the two glass sheets will be:

$$Q_{L,pred} = Q_{TOP} + Q_{BOTTOM} + Q_{sleeves} = 0.379\sigma_{SB}(T_{ABS}^4 - T_{GL,TOP}^4) + 0.149\sigma_{SB}(T_{ABS}^4 - T_{GL,BOTTOM}^4) + 2C_{sleeve}(T_{ABS} - T_{SEAL})$$

The theoretical heat loss has been predicted based on the mean absorber temperature and glass temperatures from the thermocouples positioned centrally between four pillars. The temperature field over the glass surface is discussed more fully in Moss et al. (2018c).

Measurement of emissivity on a thin sheet absorber is prone to inaccuracy because the surface is warmed by the sensor and because the distribution over the surface is being characterised in terms of points on an 8 × 8 grid. It is therefore conceivable that the above emissivities are inexact and that the actual heat loss could be modelled as a constant multiple β of the theoretical value: $Q_L = \beta Q_{L,pred}$

The net heat absorbed can be modelled as $Q_u = G(\tau\alpha) - \beta Q_{L,pred}$ giving an absorber efficiency $\eta_A = \frac{Q_u}{G} = (\tau\alpha) - \beta\left(\frac{Q_{L,pred}}{G}\right)$.

Fig. 11 shows that a straight line efficiency graph is obtained when plotting η_a against $Q_{L,pred}/G$.

The gradient of −1.09 shows the heat loss to be 9% higher than predicted. This might indicate that the mean emissivity was slightly higher than the value obtained from the emissometer point measurements. It is more likely however that there was some non-uniformity in temperature across the glass and the thermocouple readings did not accurately represent the mean temperature. The y-axis intercept (η_A = 0.744) is a measure of the transmittance-absorbance product $\tau\alpha$. This optical efficiency is higher than usually achieved by evacuated tubes since the latter suffer from a lower fill factor than flat plate collectors.

5. Conclusions

Two styles of vacuum enclosure were tested. Both performed well and demonstrated a very significant efficiency increase between ambient and evacuated conditions. 4 mm toughened glass with a 60 mm pitch pillar array provided a sufficient safety margin even when a few pillars were missing. The tray-based enclosure was more flexible than the symmetrical design and more resistant to thermal stress-induced leakage.

The symmetrical enclosure became progressively less vacuum-tight over the course of the testing. Thermal-expansion induced stresses are thought to have led to a cracking or de-bonding in the soldered joint. Cerasolzer 217 is more brittle than the indium used previously for vacuum glazing research and this makes it more prone to stress-induced leakage. A low-cost alternative to indium is highly desirable: a key requirement is sufficient mechanical strength to transmit the shear forces due to differential expansion.

The absorbers used an innovative flooded panel design with a black chrome plated coating. The concept worked well but the coating emissivity was higher than intended. The overall absorber heat loss coefficient for the final collector, U_L = 3.65 W/m^2 K, was therefore no better than typically achieved by good, non-evacuated commercial panels using high quality coatings. A collector with a high quality selective coating would achieve a significantly lower U_L and higher efficiency.

The experimental heat loss coefficient was just 9% higher than the predicted value based on measured glass and absorber temperatures. This close match indicates that the heat transfer process between absorber and glass due to a combination of radiative and low-pressure conduction effects is well understood. It therefore confirms previously published efficiency predictions for evacuated flat plate collectors.

Evacuated flat plate collectors offer significant efficiency advantages over both conventional flat plate and evacuated tube collectors. EFP collectors would gradually replace both of these conventional alternatives if a cost-effective design and manufacturing technique were available to build sealed-for-life units. The present experience with absorbers, enclosures and sealing highlights some of the challenges inherent in the development of such a product.

Acknowledgements

The authors are grateful to the Engineering and Physical Sciences Research Council (EPSRC) for funding this work as part of a collaborative programme between Warwick, Loughborough and Ulster universities, reference EP/K009915/1, EP/K010107/1 and EP/K009230/1. Matlab data and code used for the figures in this paper are openly available from http://wrap.warwick.ac.uk/95265.

References

Abbate, P., 2012. Presentation on the TVP evacuated panel at InterSolar, https://www.youtube.com/watch?v=z_4FD4Zxwew (Accessed 12/7/2017).

Alam, M., Singh, H., Suresh, S., Redpath, D.A.G., 2017. Energy and economic analysis of Vacuum Insulation Panels (VIPs) used in non-domestic buildings. Appl. Energy 188, 1–8.

Alobaid, M., Hughes, B., Calautit, J.K., O'Connor, D., Heyes, A., 2017. A review of solar driven absorption cooling with photovoltaic thermal systems. Renew. Sustain. Energy Rev. 76, 728–742.

Beikircher, T., Goldemund, G., Benz, N., 1996. Gas heat conduction in an evacuated tube solar collector. Sol. Energy 58 (4–6), 213–217.
Beikircher, T., Möckl, M., Osgyan, P., Streib, G., 2015. Advanced solar flat plate collectors with full area absorber, front side film and rear side vacuum superinsulation. Sol. Energy Mater. Sol. Cells 141, 308–406.
Benvenuti, C., Ruzinov, V., 2010. The SRB evacuated flat solar panel, Proceedings of ECOS, pp. 2–429 to 434, http://infoscience.epfl.ch/record/165003/files/Ecos2010-book2-printing.pdf?version=5.
Benvenuti, C., 2013a. The SRB solar thermal panel. Europhys News 16–18. http://dx.doi.org/10.1051/epn/2013301.
Benvenuti, C., 2013b. Particle accelerators and solar panels. Fisica E 29 (1–2), 31–38.
Benz, N., Beikircher, T., 1999. High efficiency evacuated flat-plate solar collector for process steam production. Sol. Energy 65 (2), 111–118.
Bouvier, J.-L., Michaux, G., Salagnac, P., Kientz, T., Rochier, D., 2016. Experimental study of a micro combined heat and power system with a solar parabolic trough collector coupled to a steam Rankine cycle expander. Sol. Energy 134, 180–192.
Brunold, S., Frey, R., Frei, U., A comparison of three different collectors for process heat applications. SPF publication. http://spf.ch/fileadmin/daten/publ/procheat.pdf.
Buttinger, F., Beikircher, T., Proll, M., Scholkopf, W., 2010. Development of a new flat stationary evacuated CPC-collect or for process heat applications. Sol. Energy 84, 1166–1174.
Caër, V.H.-L., De Chambriera, E., Mertina, S., Jolya, M., Schaerb, M., Scartezzinia, J.-L., 2013. Optical and morphological characterisation of low refractive index materials for coatings on solar collector glazing. Renew. Energy 53, 27–34.
Colangelo, G., Favale, E., Miglietta, P., de Risi, A., 2016. Innovation in flat solar thermal collectors: A review of the last ten years experimental results. Renew. Sustain. Energy Rev. 57, 1141–1159.
Collins, R.E., Turner, G.M., Fischer-Cripps, A.C., Tang, J.Z., Simko, T.M., Dey, C.J., Clugston, D.A., Zhang, Q.C., Garrison, J.D., 1995. Vacuum glazing – a new component for insulating windows. Build. Environ. 30 (4), 459–492.
Ehrmann, N., Reineke-Koch, R., 2012. Selectively coated high efficiency glazing for solar-thermal flat-plate collectors. Thin Solid Films 520, 4214–4218.
ETSAP, 2015. Solar Heat for Industrial Processes (IEA-ETSAP and IRENA Technology Brief E21), http://www.irena.org/DocumentDownloads/Publications/IRENA_ETSAP_Tech_Brief_E21_Solar_Heat_Industrial_2015.pdf.
Freeman, J., Hellgardt, K., Markides, C.N., 2015. An assessment of solar-thermal collector designs for small-scale combined heating and power applications in the United Kingdom. Heat Transfer Eng. 36 (14–15). http://dx.doi.org/10.1080/01457632.2015.995037.
Gao, X.-H., Theiss, W., Shen, Y.-Q., Ma, P.-J., Liu, G., 2017. Optical simulation, corrosion behavior and long term thermal stability of TiC-based spectrally selective solar absorbers. Sol. Energy Mater. Sol. Cells 167, 150–156.
Helsch, G., Deubener, J., 2012. Compatibility of antireflective coatings on glass for solar applications with photocatalytic properties. Sol. Energy 86, 831–836.
Henshall, P., Moss, R., Arya, F., Eames, P.C, Shires, S., Hyde, T., 2014. An evacuated enclosure design for solar thermal energy applications. Grand Renewable Energy 2014 (GRE2014) International Conference and Exhibition, Tokyo, Japan, 27 July – 1 August 2014, https://dspace.lboro.ac.uk/2134/16098.
Henshall, P., Eames, P., Arya, F., Hyde, T., Moss, R., Shire, S., 2016. Constant temperature induced stresses in evacuated enclosures for high performance flat plate solar thermal collectors. Sol. Energy 127, 250–261.
Incropera, F.P., DeWitt, D.P., 2002. Introduction to Heat Transfer, fourth ed. Wiley.
Joly, M., Antonetti, Y., Python, M., Gonzalez, M., Gascou, T., Scartezzini, J.-L., Schuler, A., 2013. Novel black selective coating for tubular solar absorbers based on a sol–gel method. Sol. Energy 94, 233–239.
Kalogirou, S.A., 2014. Solar Energy Engineering, second ed. Academic Press.
Kennedy, C.E., 2002. Review of mid- to high-temperature solar selective absorber materials NREL/TP-520-31267, https://www.nrel.gov/docs/fy02osti/31267.pdf.
Leone, G., Beccali, M., 2016. Use of finite element models for estimating thermal performance of façade-integrated solar thermal collectors. Appl. Energy 171, 392–404.
Lira-Cantú, M., Sabio, A.M., Brustenga, A., Gómez-Romero, P., 2005. Electrochemical deposition of black nickel solar absorber coatings on stainless steel AISI316L for thermal solar cells. Sol. Energy Mater. Sol. Cells 87, 685–694.
Lizama-Tzec, F.I., Macías, J.D., Estrella-Gutiérrez, M.A., Cahue-López, A.C., Arés, O., de Coss, R., Alvarado-Gil, J.J., Oskam, G., 2015. Electrodeposition and characterization of nanostructured black nickel selective absorber coatings for solar–thermal energy conversion. J. Mater. Sci.: Mater. Electron. 26, 5553–5561. http://dx.doi.org/10.1007/s10854-014-2195-5.
Martın, R.H., Perez-Garcıa, J., Garcıa-Soto, F.J., Lopez-Galiana, E., 2011. Simulation of an enhanced flat-plate solar liquid collector with wire-coil insert devices. Sol. Energy 85, 455–469.
McDonald, G.E., 1975. Spectral reflectance properties of black chrome for use as a solar selective coating. Sol. Energy 17, 119–122.
Moss, R., Shire, S., 2014. Design and performance of evacuated solar collector micro-channel plates. In: Conference Proceedings: EuroSun 2014, Aix-les-Bains (France), 16–19 September 2014, http://proceedings.ises.org/paper/eurosun2014/eurosun2014-0039-Moss.pdf.
Moss, R.W., Shire, G.S.F., Henshall, P., Eames, P.C., Arya, F., Hyde, T., 2017. Optimal passage size for solar collector micro-channel and tube-on-plate absorbers. Sol. Energy 153, 718–731. http://dx.doi.org/10.1016/j.solener.2017.05.030.
Moss, R.W., Henshall, P., Arya, F., Shire, G.S.F., Hyde, T., Eames, P.C., 2018a. Performance and operational effectiveness of evacuated flat plate solar collectors compared with conventional thermal, PVT and PV panels. Appl. Energy 216, 588–601. http://dx.doi.org/10.1016/j.apenergy.2018.01.001.
Moss, R.W., Shire, G.S.F., Henshall, P., Eames, P.C., Arya, F., Hyde, T., 2018b. Design and fabrication of a hydro-formed absorber for an evacuated solar collector. Appl. Therm. Eng.
Moss, R.W., Shire, G.S.F., Eames, P.C., Henshall, P., Hyde, T., Arya, F., 2018c. Design and commissioning of a virtual image solar simulator for testing thermal collectors. Sol. Energy 159, 234–242. http://dx.doi.org/10.1016/j.solener.2017.10.044.
Nkwetta, D.N., Smythe, M., 2012. The potential applications and advantages of powering solar air-conditioning systems using concentrator augmented solar collectors. Appl. Energy 89, 380–386.
O'Hegarty, R., Kinnane, O., McCormack, S.J., 2017. Concrete solar collectors for façade integration: An experimental and numerical investigation. Appl. Energy 206, 1040–1061.
Purohit, I., Purohit, P., 2017. Technical and economic potential of concentrating solar thermal power generation in India. Renew. Sustain. Energy Rev. 78, 648–666.
Riggs, B.C., Biedenharn, R., Dougher, C., Ji, Y.V., Xu, Q., Romanin, V., Codd, D.S., Zahler, J.M., Escarra, M.D., 2017. Techno-economic analysis of hybrid PV/T systems for process heat using electricity to subsidize the cost of heat. Appl. Energy 208, 1370–1378.
Selvakumar, N., Barshilia, H.C., 2012. Review of physical vapor deposited (PVD) spectrally selective coatings for mid- and high-temperature solar thermal applications. Sol. Energy Mater. Sol. Cells 98, 1–23.
Sharma, N., Diaz, G., 2011. Performance model of a novel evacuated-tube solar collector based on minichannels. Sol. Energy 85, 881–890.
SPF catalogue of solar collector test results http://www.spf.ch/index.php?id=111&L=6 accessed August 2017.
TVP Solar, MT-30 datasheet, http://www.tvpsolar.com/files/pagine/1464011780_MT-Power%20Datasheet%20(v4.2x)(ver5).pdf (Accessed 12/7/2017).
Suman, S., Khan, M.K., Pathak, M., 2015. Performance enhancement of solar collectors – a review. Renew. Sustain. Energy Rev. 49, 192–210.
Simko, T.M., Fischer-Crips, A.C., Collins, R.E., 1998. Temperature-induced stresses in vacuum-glazing: modelling and experimental validation. Sol. Energy 63 (1), 1–21.
Zambolin, E., Col, D.D., 2010. Experimental analysis of thermal performance of flat plate and evacuated tube solar collectors in stationary standard and daily conditions. Sol. Energy 84, 1382–1396.